Journal of Thermal Analysis and Calorimetry (2020) 139:3395–3403
https://doi.org/10.1007/s10973-019-08705-8

Effects of fly ash microspheres on sulfate erosion resistance and chlorion penetration resistance in concrete

Xueming Wang[1] · Jun Yuan[1] · Peng Wei[1] · Mengwei Zhu[1]

Received: 1 May 2019 / Accepted: 15 August 2019 / Published online: 5 September 2019

Abstract

Fly ash microsphere (FAM) is a superfine fly ash product consisting of perfectly spherical and smooth particles. In this study, FAM was added to concrete for use in saline soil areas. The replacement levels of cement by FAM were 10% and 20% with a water-to-binder (*w*/*b*) ratio of 0.42. The hydration heat, thermogravimetric (TG) analysis, rheological performance, and the flowability of pure cement (CF0) and FAM-doped cement (CF10 and CF20) were investigated. The second exothermic peak occurred earlier and was higher in the FAM-doped cement than the CF0. The results showed that the nucleation effect of the FAM accelerated the early hydration speed of the cement. The TG results indicated that the $Ca(OH)_2$ consumption was higher at 28 days due the addition of the FAM, which improved the interfacial transition zone and blocked the connected porosity of the hardened cement paste. The ball-bearing effect of the FAM particles in the paste reduced the internal friction between the grains, thereby significantly improving the rheology and the flowability of the cement paste. In addition, the filler effect of the FAM particles significantly improved the pore structure, which increased the compressive strength and chlorion penetration of the concrete. It was also found that the FAM increased the workability while improving the resistance of the concrete to sulfate attack when exposed to multiple drying–wetting cycles.

Keywords Fly ash microsphere · Saline soil · Chlorion penetration · Sulfate attack · Drying–wetting cycles

Introduction

Saline soil is characterized by a high content of soluble salts (> 0.3%) [1]. In regions with saline soil, many concrete structures are severely deteriorated due to the dissolution of soluble salts such as sulfate or chloride [2–4]. The corrosion of concrete structures in saline soil areas is a complex physicochemical process [5]. The physical salt attack of ions leads to surface cracking and scaling of concrete [6], resulting in negative effects on the durability and the safety of concrete structures [7]. The chemical attack consists of reactions between the ions and the cement hydration products [8]. The accumulation of corrosion products increases the swelling pressure, resulting in cracking, spalling, and strength loss of the concrete [9]. Previous research has shown that chloride attacks tend to be accelerated by sulfate ions [10]. Hence, it is important to investigate the damage process of concrete in saline soil areas.

Unfortunately, saline soils are widely distributed in northwestern China due to the harsh climate; this results in poor construction conditions. The service environment of concrete structures strongly affects the properties and service life of the structures. The concrete is often mixed insufficiently, and early age curing may not be adequate due to water shortages and poor construction conditions. Under these conditions, the macro- and microproperties of the concrete are strongly affected, thereby accelerating the diffusion of harmful ions. Therefore, sulfate erosion and chloride ion penetration occur and thus affect the durability of the concrete [11–13]. It is generally accepted that the addition of mineral admixtures enhances the erosion resistance of concrete. However, Zhang et al. [12] found that under insufficient initial moist curing, the incorporation of fly ash (FA) and ground granulated blast-furnace slag (GGBS) contributed little to improving the resistance of concrete to sulfate attack. Therefore, under harsh

✉ Jun Yuan
1203858237@qq.com

[1] Northwest Electric Power Design Institute Co., Ltd. of China Power Engineering Consulting Group, Xi'an 710075, China

conditions, high mineral admixture contents have limited influence on the resistance of concrete to sulfate attack and chloride ion penetration. As a result of above facts, more attention should be paid to the workability of concrete. The workability of freshly mixed concrete is an important indicator of quality in concrete construction.

Fly ash microsphere (FAM) is a superfine fly ash product collected from the exhaust smoke of coal-fired power plants [14] with spherical particles of micrometer scale size. Previous studies [14–16] have shown that the incorporation of ultrafine fly ash improved the workability of concrete. There are three reasons for incorporating FAM in concrete: (1) the first reason is the filler effect [17]. The particle size of FAM is very small with a mean particle diameter of 1–5 microns; the particles fill the interstitial voids, thereby releasing entrapped water in the voids between the cement grains without increasing the surface area. (2) The second reason is the 'ball-bearing' effect [18]; the FAM particles are spherical, have a smooth surface, and operate similar to ball bearings, thereby improving the rheology of cementitious suspensions [19]. (3) The third reason is the water-reducing effect [20]. FAM has a high calcium content, high surface activity, and low water adsorption and acts as a water reduction and lubrication agent in concrete. These properties make FAM a suitable admixture for concrete used in saline soil regions due to the physical and chemical effects including a change in the microstructure, filling of pores, reducing the water used, and improving the workability. Previous studies have evaluated the feasibility of using FAM in concrete; the results indicated that FAM solves several technical problems associated with ordinary concrete. Kwan et al. [14], Chen et al. [17], Kwan and Li [21], and Yang et al. [22] reported that FAM acted as an inorganic dispersion agent and had a filler effect, which improved the workability of cement, mortar, or concrete. Other research [19, 23] has found that the particle geometry had a significant impact on the rheological properties because the spherical particles reduced the yield stress or plastic viscosity of the fresh cement paste. Hence, FAM minimizes the loss of workability of concrete over time.

However, concrete used in saline soil areas must possess not only good workability in the fresh state but also excellent mechanical properties and durability. Previous studies [18, 21] have reported that FAM was capable of densifying the pore structure and increasing the particle packing density, which improved the concrete performance. In addition, the pozzolanic reaction of the FAM improved the microstructure of the hydration products and increased the durability of concrete [18]. Herein, it is proposed that FAM may be a suitable material to be added to concrete in saline soil regions. We investigated the effect of FAM in the hydration and hardening periods of the FAM-blended cement pastes and researched the chloride penetration and resistance to sulfate attack of the FAM-blended cement concrete.

Experimental

Raw materials

The cement was ordinary Portland cement (OPC) with a strength grade of 42.5 and conformed to the Chinese National Standard GB 175-1999. The FAM was supplied by Daote Technology Co. Ltd (Shenzhen, China) and had been tested to comply with the Chinese National Standard GB/T 1596-2005: fly ash used for cement and concrete. The chemical compositions of the OPC and FAM are shown in Table 1. Figure 1a shows the particle size distributions of the OPC and FAM. The FAM had a $d_{(0.5)}$ of 1.138 μm (superfine powder); therefore, aggregates (the second peak of the FAM in Fig. 1a) are easily formed. The scanning electron microscope (SEM) image of the surface of the FAM particles is shown in Fig. 1b. It is observed that the FAM particles have a perfect spherical shape and the aggregates can also be seen.

Mix proportions

Tables 2 and 3 list the mix proportions of the paste and concrete samples, respectively. The replacement levels of the cement by the FAM were 0, 10%, and 20% by mass. The water-to-binder (w/b) ratio of all the paste and concrete specimens was 0.42. The three groups of specimens are named CF0, CF10, and CF20, respectively.

Test methods

The heat evolution of the three mixture samples (listed in Table 2) was measured using a TAM Air Calorimeter at 25 °C for a period of 72 h. The hydration heat results represent the early hydration activity of the samples.

Thermogravimetric (TG) analysis of the three mixture samples (listed in Table 2) was conducted with a constant heating rate of 10 °C per min from 30 to 900 °C under a nitrogen atmosphere flow. The contents of the hydration products calcium hydroxide ($Ca(OH)_2$) were calculated

Table 1 Chemical compositions of raw materials (%)

Composition	SiO_2	Al_2O_3	Fe_2O_3	CaO	MgO	SO_3	LOI
OPC	21.10	6.33	4.22	54.86	2.6	2.66	2.42
FAM	47.79	16.10	7.21	18.71	1.46	0.13	0.75

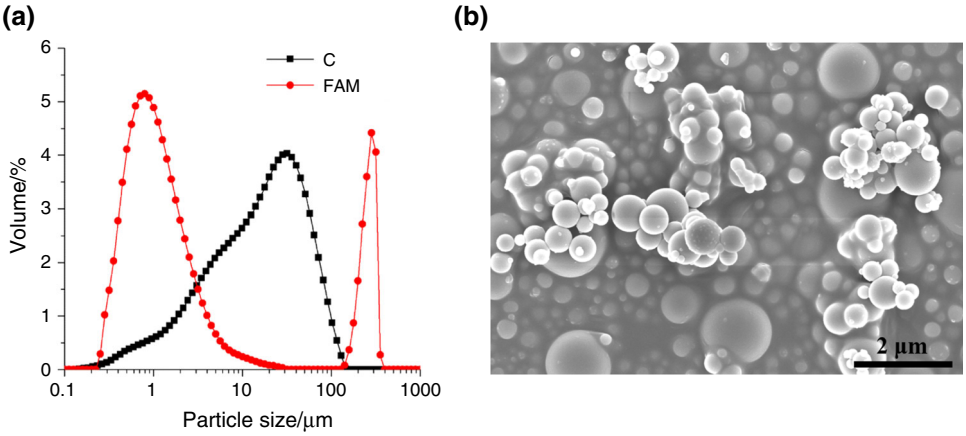

Fig. 1 **a** Particle size distribution of cement and FAM and **b** the SEM images of the FAM

Table 2 Mix proportions of the paste samples

Samples	OPC/by mass%	FAM/by mass%	Water-to-binder ratio
CF0	100	0	0.42
CF10	90	10	0.42
CF20	80	20	0.42

Table 3 Mix proportions of the concrete samples (kg m^{-3})

Samples	OPC	FAM	Water	Fine aggregate	Coarse aggregate
CF0	350	0	147	837	1066
CF10	315	35	147	837	1066
CF20	280	70	147	837	1066

from the TG/differential TG (DTG) curve at ages of 3 and 28 days, respectively.

The rheology of the three fresh pastes (listed in Table 2) was evaluated with a rotor rheometer. The cup of the rheometer was filled with the paste, and the measurement was conducted according to the set program. The shear rates applied to the samples were 25, 50, 75, 100, 125, 150, 175, 200, 225, and 250 (s^{-1}). First, pre-shearing was applied from 25 to 250 s^{-1} for 90 s, followed by data-logging from 250 to 0 s^{-1}, which lasted 108 s. A computer monitoring system was used to capture the data during testing. According to the Bingham fluid model, as shown in the following equation:

$$\tau = \tau_0 + \eta \cdot \gamma$$

the yield stress (τ_0) and plastic viscosity (η_p) of the fresh pastes were calculated, where τ is the shear stress (Pa) and γ is the shear rate (s^{-1}).

The fluidity of the fresh pastes was determined according to the Chinese Standard GB/T 8077-2012: methods for testing uniformity of concrete admixture. After mixing, a flow cone (60 mm height, 36 mm top diameter, and 60 mm bottom diameter) in the center of a glass plate was used to fill the fresh pastes. Subsequently, the flow cone was vertically removed from the glass plate and the maximum diameter of the spread sample was measured.

The collapsed slump of the concrete samples (listed in Table 3) was tested with a mini-slump instrument according to the Chinese Standard GB/T 50080-2016: standard for test method of performance on ordinary fresh concrete. An equal amount of superplasticizer (5.6 kg m^{-3}) was added to each sample to adjust the concrete flowability. The collapsed slump of the concrete samples was measured three times, i.e., immediately after mixing was completed, after half an hour, and after 1 h.

Concrete cubes (listed in Table 3) were prepared with a dimension of 100 × 100 × 100 mm. All the samples were cured at a constant temperature and humidity (20 °C, higher than 95% RH). At ages of 28 and 90 days, the compressive strengths of the concrete cubes were tested.

The current passing through the concrete over a period of 6 h was measured according to ASTM C1202 'Standard test method for electrical indication of the concrete ability to resist chloride ion penetration.' The chloride ion permeability of the concrete at ages of 28 and 90 days was evaluated by using a chlorine ion penetration level.

The concrete samples cured for 28 days were immersed in 5% sodium sulfate (Na_2SO_4) solution and were exposed to drying–wetting cycles to evaluate the sulfate resistance of the concrete samples. According to the Chinese Standard GB/T 50082-2009: standard for test methods of long-term performance and durability of ordinary concrete, the wetting–drying cycle was implemented as follows: (1) immersion in 5% sodium sulfate solution at 20 °C for 15 h, (2) natural drying for 1 h, (3) oven drying at 80 °C for 6 h, and (4) natural cooling for 2 h. The concrete samples were exposed to this cycle 90 and 120 times, respectively. Finally, the compressive strength of the concrete cubes was tested after the drying–wetting cycles. The corrosion resistance coefficient (K_f) is defined as:

$$K_f = \frac{f_{cn}}{f_{c0}} \times 100\%$$

where f_{cn} is the compressive strength of the samples exposed to sulfate attack and f_{c0} is the compressive strength of the control group (the 28 days compressive strength of the samples).

Results and discussion

Hydration heat of the pastes

Figure 2a, b shows the exothermic rate and hydration heat curves of the three pastes, respectively. As shown in Fig. 2a, the exothermic rate curves of all the samples were in agreement with the five stages of cement hydration [24]. The replacement of 10% and 20% of the cement by the FAM did not result in the disappearance or appearance of additional peaks; however, the intensity and the timing of the second peak were different. Compared with CF0, the second peaks of CF10 and CF20 occurred slightly earlier and the intensities were slightly higher. This indicates that the replacement of the cement by FAM accelerated the early hydration speed of the cement. This may be attributed to two reasons. First, because the FAM has a micrometer scale particle size, on the one hand, this provides growth sites for the hydration products and promotes nucleation; on the other hand, it provides more growing space for cement hydration. Second, the FAM increases the effective *w/b* ratio of the hydration process to improve the early hydration of cement [18]. Figure 2b illustrates the cumulative heat release of the samples. The total hydration heat released from the three samples over 72 h was 288.08, 275.96, and 260.20 J g^{-1}, respectively. Compared to CF0, as the dosage of FAM increased from 10 to 20%, the total heat release decreased by 4.2% (less than 10%) and 9.7% (much less than 20%), respectively. This further confirms the accelerating effect of the FAM on the cement hydration.

The literature indicates that the hydration characteristics of GGBS and FA-blended cement pastes have been investigated widely. The replacement of cement by GGBS delays the early hydration and some parts of the reaction and, therefore, affects the second exothermic peak (which would be delayed) [25]. The main active substance of the fly ash, namely siliceous–aluminous vitreum, is wrapped in a water film layer during the early stages of hydration, thereby reducing its activity. Hence, the replacement of cement by FA delays early hydration [26, 27]. At the same *w/b* ratio, there are stricter requirements for the curing condition of concrete containing FA or GGBS than FAM.

Thermogravimetric (TG) analysis

The TG/DTG curves are shown in Figs. 3a, b at ages of 3 and 28 days, respectively. As shown in Fig. 3, an endothermic peak of each sample is observed in the DTG curves at approximately 300–500 °C, which denotes the decomposition of $Ca(OH)_2$. On the one hand, the replacement of cement by FAM accelerated the early hydration of cement (as depicted in the hydration heat results) and increased the $Ca(OH)_2$ content; on the other hand, the pozzolanic reaction of the FAM consumed $Ca(OH)_2$ in the cement–FAM system. The total amount of $Ca(OH)_2$ was then calculated (listed in Table 4) to investigate the effect of FAM on the cement hydration process [28]. The following equation was used to determine the $Ca(OH)_2$ content (%):

$$Ca(OH)_2 \text{ content } \% = 74.09/18.01 \times (W_{300} - W_{600})\,\%$$

where W_{300} and W_{600} are the sample mass percent (%) recorded during the TGA tests at $T = 300$ °C and $T = 600$ °C, respectively. The ratio (74.09/18.01) corresponds to the molar mass ratio of $Ca(OH)_2$ and H_2O.

As shown in Table 4, the $Ca(OH)_2$ content of CF10 was slightly higher than that of CF0 at 3 days (the increased value of 3.3%). However, the $Ca(OH)_2$ content of CF20 was lower than that of CF0 at 3 days (a decrease of 9.9%).

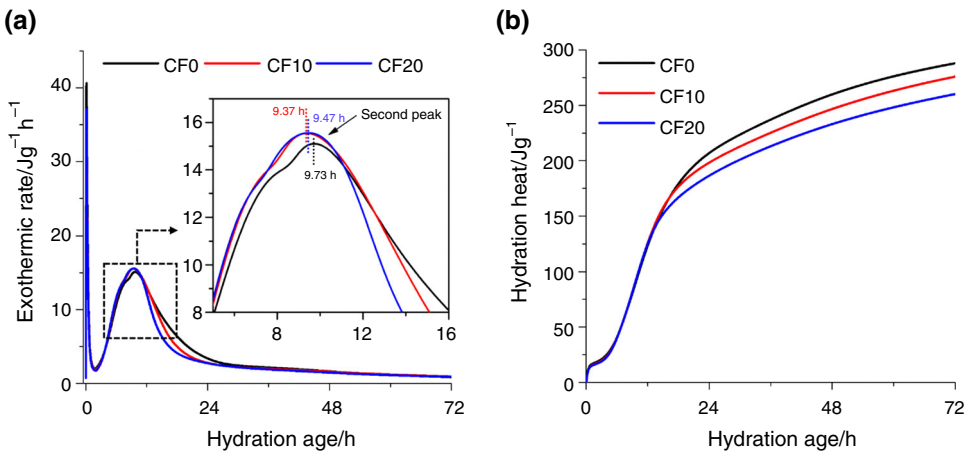

Fig. 2 **a** Exothermic rate curves and **b** cumulative heat curves of the binders during hydration

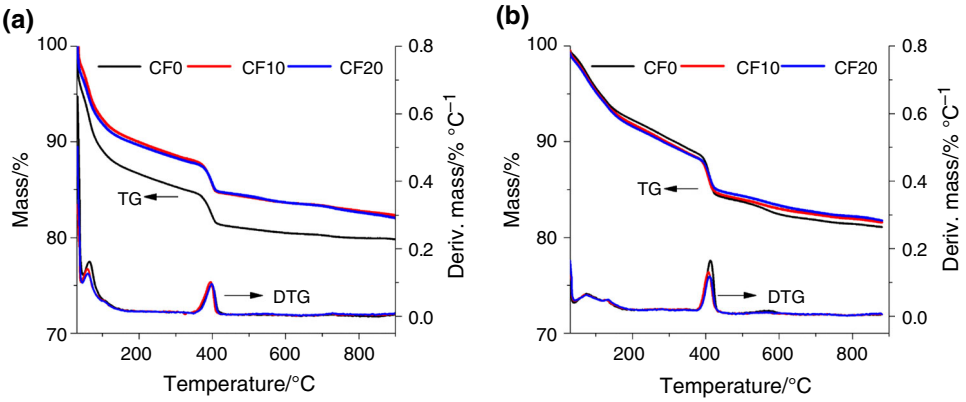

Fig. 3 TG/DTG curves of the hardened pastes at the ages of **a** 3 and **b** 28 days

Table 4 The content of $Ca(OH)_2$ in the hardened pastes at 3 and 28 days

Samples	$Ca(OH)_2$ content/%	
	3 days	28 days
CF0	14.00	22.78
CF20	14.46	20.48
SF10	12.61	17.94

The $Ca(OH)_2$ content of the FAM-doped samples did not decrease at 3 days. These results indicated that FAM accelerates the early hydration speed of the cement. Therefore, the total $Ca(OH)_2$ content of the FAM-doped cement samples did not decrease as the cement content decreased (reducing the amount of $Ca(OH)_2$) and the reaction of FAM (consuming $Ca(OH)_2$). While, from 3 to 28 days, the $Ca(OH)_2$ content of all samples increased, which indicated that the hydration degree of the cement increased from 3 to 28 days. The $Ca(OH)_2$ contents of CF10 (a decrease of 10.1%) and CF20 (a decrease of 21.2%) were lower than that of CF0 at 28 days. This shows that the amount of $Ca(OH)_2$ consumed by the pozzolanic reaction of FAM was slightly larger than that generated by cement hydration during 28 days, which may reduce the mean size of the $Ca(OH)_2$ crystals and result in a denser microstructure of the interfacial transition zone (ITZ) at later ages.

Rheological property and fluidity of the pastes

The rheological performance and the initial fluidity of the fresh pastes (listed in Table 2) were tested. The typical flow curves of the shear rate versus the shear stress are shown in Fig. 4a. The shear rates applied to the samples were 25, 50, 75, 100, 125, 150, 175, 200, 225, and 250 (s^{-1}). First, pre-shearing was applied from 25 to 250 s^{-1} for 90 s, followed by data-logging from 250 to 0 s^{-1}, which lasted 108 s. The data shown in the shear rate versus shear stress curves were fitted to the Bingham model. The yield stress (τ_0) and the plastic viscosity (η) of the paste samples are shown in the table in Fig. 4. The yield stress of the pastes decreased, but the plastic viscosity increased with the FAM content increasing from 0 to 20%. The spherical shape of the FAM particles reduced the internal friction between the grains and the 'ball-bearing' effect of the FAM particles decreased the attraction forces generated between the cement grains, thus reducing the yield stress. The plastic viscosity of the fresh pastes was mainly influenced by the competition between the increasing free water and increasing specific surface area caused by the FAM. With the addition of the FAM, on the one hand, the overall solid surface area increased, thereby reducing the water film thickness (WFT) and increasing the plastic viscosity. On the other hand, the lubricating effect of the FAM particles released the trapped free water in the aggregates, which decreased the plastic viscosity and increased the WFT. It appeared that the increase in the specific surface area was the dominant factor, resulting in a decrease in the WFT and thus an increase in the plastic viscosity. Kwan et al. [14] found that when the *w/b* ratio was less than 0.28, as the FAM content increased, the WFT decreased; in other words, the replacement of cement by FAM increased the WFT only at relatively low *w/b* ratio.

The fluidity of the fresh pastes was assessed, as shown in Fig. 4b; the flow spread results are shown in the table. As the FAM content increased, the initial fluidity increased. This result is attributed to the spherical shape and smoothness of the FAM particles, which reduced the interparticle friction between the rough grains. Both the rheology and the flowability were improved by the addition of the FAM to the cement pastes.

Effects of FAM on the collapsed slump of concrete

The concrete collapsed slump results are shown in Table 5. At the same test time, the diameter of the collapsed slump of concrete increased as the FAM dosage increased. The FAM concrete exhibits considerably better workability

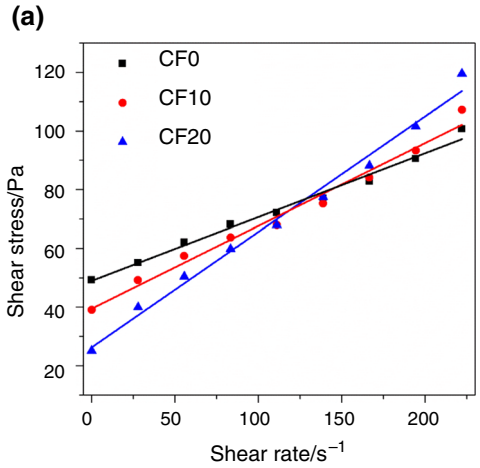

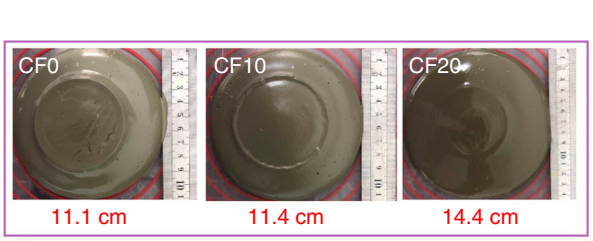

Experimental data

Samples	τ0/Pa	η/Pa s	Flow spread/cm
CF0	48.97	0.22	11.1
CF10	39.47	0.28	11.4
CF20	26.27	0.40	14.4

Fig. 4 **a** Flow curves of the pastes and **b** flow spread of the pastes

Table 5 The collapsed slump of concrete (cm)

Samples	Immediately after mixing completed	Half an hour later	1 hour later
CF0	16.4	14.7	12.9
CF10	17.6	17.2	16.3
CF20	19.2	18.4	17.6

than the OPC concrete (19.2-cm initial slump for CF20 concrete compared with 16.4-cm initial slump for OPC concrete). For each sample, the collapsed slump decreased during the measuring period. The rates of concrete slump-loss of CF0, CF10, and CF20 were equal to 3.5 cm h^{-1}, 1.3 cm h^{-1}, and 1.6 cm h^{-1}, respectively. These results indicate that the FAM improved the flowability and slump-loss resistance of the concrete. This is attributed to the micron-sized particles of the FAM, which filled the voids and released the trapped water between the cement grains. [21]. In addition, the 'ball bearing' and the 'water-reducing' effects of the FAM provided lubrication to improve the workability of the concrete.

Compressive strength

Figure 5 shows the compressive strength results of the concrete samples at the ages of 28 and 90 days, respectively. The compressive strengths of the concrete samples containing FAM were higher than that of the OPC concrete. At the same age, the compressive strength increased slightly with the increase in the FAM content. These results show that the replacement of cement by FAM has an effect on the compressive strength of the concrete. It has been reported that FAM improved the compressive strength at a later age [18]. This result is due to the accelerating effect of

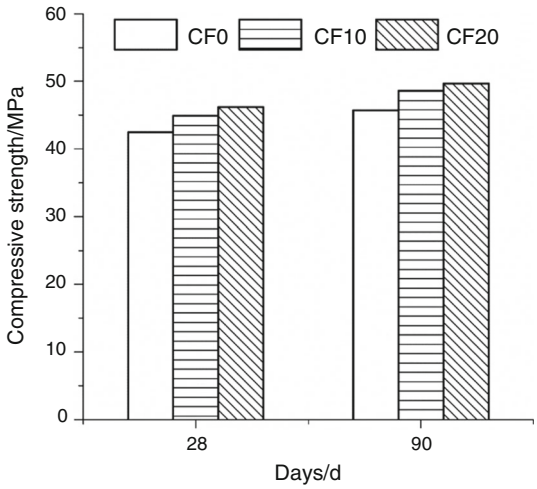

Fig. 5 Compressive strength of concretes

the FAM on the early cement hydration; in addition, the FAM reaction consumes $Ca(OH)_2$, which improves the microstructures, especially in the ITZ. However, when the FAM content was increased from 10 to 20%, the increase in the compressive strength was not significant (3% for 28 days and 2% for 90 days). This was probably the result of decreasing the cement content and the limited effect of the FAM on the compressive strength. Therefore, considering the cost of the material, the appropriate dosage of FAM should be 10%.

Chloride ion permeability of concrete

Figure 6 displays the results of passing a current through the concrete samples for 6 h at the ages of 28 and 90 days. The chloride ion permeability levels of the FAM-doped concrete samples were one level lower than that of the OPC concrete. This result indicates that the FAM-blended

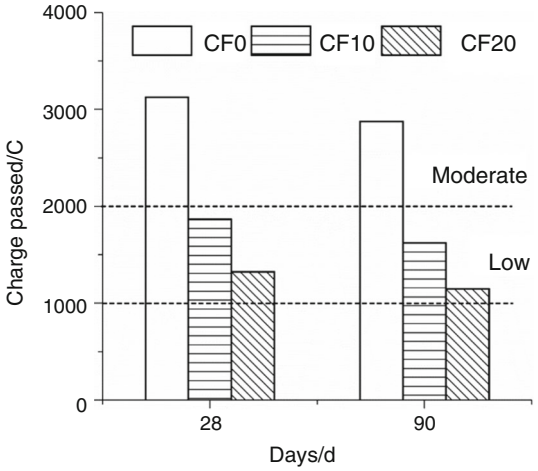

Fig. 6 Chloride ion permeability of the concretes at 28 and 90 days

concrete samples exhibited good resistance to chloride penetration. The pozzolanic reaction of the FAM consumes $Ca(OH)_2$, which is produced by cement hydration; the ITZ was improved and most of the connected pores were blocked by the reaction products, resulting in better compactness of the FAM-based concrete. As the FAM content increased from 10 to 20%, the charge passed decreased. This was probably due to the larger amount of $Ca(OH)_2$ that was consumed as the FAM content increased, which decreased the connected porosity.

Sulfate attack

Plotted in Fig. 7a, b are the compressive strength and corrosion resistance coefficients of the concrete cubes exposed to 90 and 120 drying–wetting cycles, respectively. The compressive strength of the concrete samples after the drying–wetting cycles was lower than that at the age of 28 days (as shown in Fig. 5). When the Na_2SO_4 solution comes into contact with the concrete cube, a sulfate attack occurs due to the following processes. First, sulfate ions enter the concrete cube and diffuse through the pores. Because there is a concentration gradient in the pore network between the inside and outside of the concrete cube, the sulfate attack occurs from the high to the low concentration zones. Second, chemical reactions take place between the sulfate ions and the cement matrix [29]. The corrosion resistance coefficient of the FAM-based concrete was higher than that of the OPC sample, which indicated that the addition of the FAM significantly improved the sulfate resistance of the concrete. This occurred because the second hydration effect increased due to the addition of the FAM and the reaction products filled the interior of the concrete, which blocked the connected pores and inhibited the ion transportation. The chloride ion permeability results also indicate that the FAM enhanced the compactness of the concrete, which increased the resistance to ion attack after the drying–wetting cycles. As the FAM content increased from 10 to 20%, the corrosion resistance coefficients increased only slightly. The corrosion resistance coefficients of the FAM-based concrete were very high (approaching 100%) after 90 drying–wetting cycles, which occurred because the compressive strength of the FAM-based concrete was high at the longer curing age. Still, it is important to note that the damage progresses from the outside to the interior of the concrete and was not sufficient to break the concrete after 90 drying–wetting cycles. Therefore, the results observed after the 90 drying–wetting cycles should not be used to determine the sulfate attack resistance of the concrete.

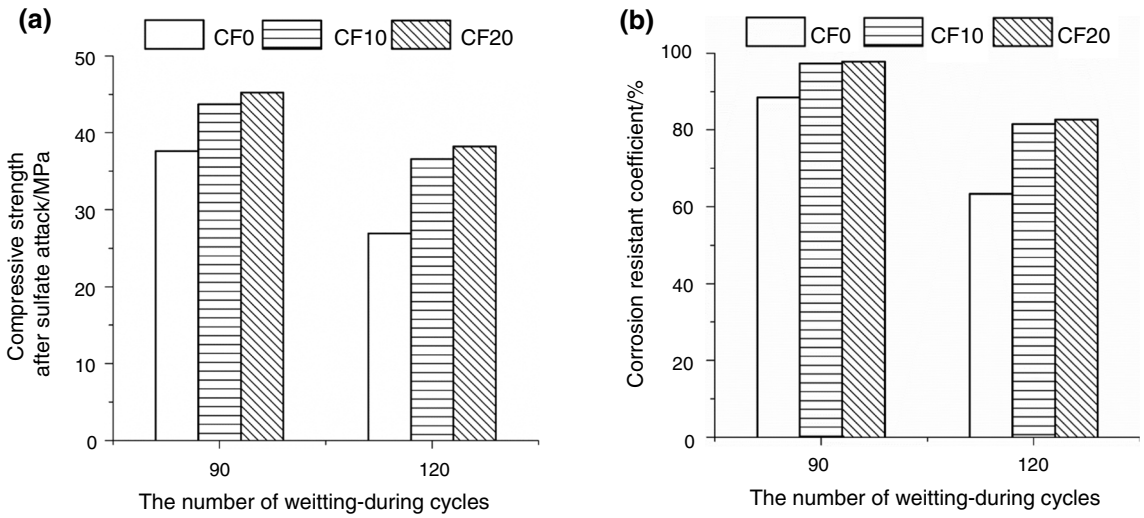

Fig. 7 **a** The compressive strength and **b** the corrosion resistance coefficient of concrete exposed to the sulfate solution after 90 and 120 wetting–drying cycles

Conclusions

1. The replacement of cement by the FAM accelerated the early hydration speed of the cement. The TG results showed that the pozzolanic reaction of the FAM progressed significantly in the later stage and consumed large amounts of $Ca(OH)_2$, which improved the ITZ and blocked the connected porosity. In addition, the FAM particles acted as 'ball bearings' in the pastes to reduce the internal friction between the grains, thereby significantly improving the rheology and the flowability of the cement paste.
2. The FAM-based concrete exhibited considerably better workability than the OPC concrete at the time of mixing and better slump-loss resistance over 1 h. The FAM-based concrete showed higher late-age compressive strength and better resistance to chloride ion penetration than the OPC concrete. The small particle size and high sphericity of the FAM result in a good 'filler effect' and 'water-reducing effect.' Therefore, the addition of FAM enhanced the compactness and improved the flowability of the concrete.
3. The FAM-based concrete exhibited better resistance to sulfate attack than the OPC concrete after being exposed to the wetting–drying cycles. The presence of the FAM resulted in the consumption of large amounts of $Ca(OH)_2$ which can improve the microstructure and the resistance to ion ingression, and then resulted in greater durability of the FAM-based concrete.
4. In practical applications, thorough mixing and sufficient curing of concrete in saline soil areas can be problematic. Hence, the FAM has a great potential as a cementitious filler because it improves the workability and durability of concrete.

References

1. Zhuang SY, Wang Q, Zhou YQ. Research on the resistance to saline soil erosion of high-volume mineral admixture steam-cured concrete. Constr Build Mater. 2019;202:1–10.
2. Pasupathy K, Berndt M, Sanjayan J, Rajeev P, Cheema DS. Durability of low-calcium fly ash based geopolymer concrete culvert in a saline environment. Cem Concr Res. 2017;100:297–310.
3. Neville A. The confused world of sulfate attack on concrete. Cem Concr Res. 2004;34:1275–96.
4. Chen F, Gao JM, Qi B, Shen DM, Li LY. Degradation progress of concrete subject to combined sulfate–chloride attack under drying–wetting cycles and flexural loading. Constr Build Mater. 2017;151:164–71.
5. Nie LX, Xu JY, Bai E. Dynamic stress–strain relationship of concrete subjected to chloride and sulfate attack. Constr Build Mater. 2018;165:232–40.
6. Wang DZ, Zhou XM, Fu B, Zhang LR. Chloride ion penetration resistance of concrete containing fly ash and silica fume against combined freezing–thawing and chloride attack. Constr Build Mater. 2018;169:740–7.
7. Shi MX, Wang Q, Zhou ZK. Comparison of the properties between high-volume fly ash concrete and high-volume steel slag concrete under temperature matching curing condition. Constr Build Mater. 2015;98:649–55.
8. Lorente S, Pierre M, Cubaynes Y, Auger J. Sulfate transfer through concrete: migration and diffusion results. Cem Concr Compos. 2011;33:735–41.
9. Ferraris CF, Stutzman PE, Snyder KA. Sulfate resistance of concrete: a new approach. R&D serial no. 2486. Skokie: Portland Cement Association; 2006.
10. Liu GJ, Zhang YS, Ni ZW, Huang R. Corrosion behavior of steel submitted to chloride and sulphate ions in simulated concrete pore solution. Constr Build Mater. 2016;115:1–5.
11. Abdelmseeh VA, Jofriet J, Hayward G. Sulphate and sulphide corrosion in livestock buildings, part I: concrete deterioration. Biosyst Eng. 2008;99:372–81.
12. Zhang ZQ, Wang Q, Chen HH, Zhou YQ. Influence of the initial moist curing time on the sulfate attack resistance of concretes with different binders. Constr Build Mater. 2017;144:541–51.
13. Wang Q, Wang DQ, Zhuang SY. The soundness of steel slag with different free CaO and MgO contents. Constr Build Mater. 2017;151:138–46.
14. Kwan AKH, Chen JJ. Adding fly ash microsphere to improve packing density, flowability and strength of cement paste. Powder Technol. 2013;234:19–25.
15. Collins F, Sanjayan JG. Effects of ultra-fine materials on workability and strength of concrete containing alkali-activated slag as the binder. Cem Concr Res. 1999;29:459–62.
16. Shaikh FUA, Supit SWM. Compressive strength and durability properties of high volume fly ash (HVFA) concretes containing ultrafine fly ash (UFFA). Constr Build Mater. 2015;82:192–205.
17. Chen JJ, Ng PL, Li LG, Kwan AKH. Production of high-performance concrete by addition of fly ash microsphere and condensed silica fume. Procedia Eng. 2017;172:165–71.
18. Wang Q, Wang DQ, Chen HH. The role of fly ash microsphere in the microstructure and macroscopic properties of high-strength concrete. Cem Concr Compos. 2017;83:125–37.
19. Laskar AI, Talukdar S. Rheological behavior of high performance concrete with mineral admixtures and their blending. Constr Build Mater. 2008;22:2345–54.
20. Sun W, Yan HD, Zhan BG. Analysis of mechanism on water-reducing effect of fine ground slag, high-calcium fly ash, and low-calcium fly ash. Cem Concr Res. 2003;33:1119–25.
21. Kwan AKH, Li Y. Effects of fly ash microsphere on rheology, adhesiveness and strength of mortar. Constr Build Mater. 2013;42:137–45.
22. Yang T, Zhua HJ, Zhang ZH, Gao X, Zhang CS, Wu QS. Effect of fly ash microsphere on the rheology and microstructure of alkali-activated fly ash/slag pastes. Cem Concr Res. 2018;109:198–207.
23. Provis JL, Duxson P, Deventer JSJV. The role of particle technology in developing sustainable construction materials. Adv Powder Technol. 2010;21:2–7.
24. Sun JF, Shen XD, Tan G, Tanner JTE. Compressive strength and hydration characteristics of high-volume fly ash concrete prepared from fly ash. J Therm Anal Calorim. 2019;136:565–80.
25. Escalante JI, Gomez LY, Johal KK, Mendoza G, Mancha H, Méndeza J. Reactivity of blast-furnace slag in Portland cement blends hydrated under different conditions. Cem Concr Res. 2001;31(10):1403–9.
26. Wczelik WN. Heat evolution in hydration cementitious systems admixture with fly ash. J Therm Anal Calorim. 2001;65:613–9.

27. Han FH, Zhang ZQ, Liu JH, Yan PY. Hydration kinetics of composite binder containing fly ash at different temperatures. J Therm Anal Calorim. 2016;124:1691–703.
28. Feng JJ, Liu SH, Wang ZG. Effects of ultrafine fly ash on the properties of high-strength concrete. J Therm Anal Calorim. 2015;121:1213–23.
29. Collepardi M. A state-of-the-art review on delayed ettringite attack on concrete. Cem Concr Compos. 2003;25:401–7.